Project 1: Scattering of H atoms on a Kr atom

Mione Filippo, Rigo Mauro, Slongo Francesco

March 30, 2020

University of Trento
Department of Physics
Via Sommarive, 14, 38123 Povo
Trento, Italy

Abstract

We studied the bound states of a harmonic oscillator in 1D and 3D and the total cross section of a scattering with a (12, 6) Lennard-Jones potential. The numerical energies and wave functions of the bound states are correct and we obtained a power law with exponent 4 for the behaviour of the error as a function of the mesh step, as expected for the Numerov algorithm. The total cross section that we calculated predicts correctly the presence of three quasibound states. The obtained values for the energies of these states are systematically lower, but compatible with the experimental ones within 3σ.

1 Introduction to the physical problem

The purpose of the following work is to numerically solve the stationary Schrödinger Equation (SE) to calculate the total cross section for the scattering between H and Kr atoms.

The wave function of a quantum-mechanical system corresponding to a stationary state must solve the time-independent Schrödinger equation:

$$-\frac{\hbar^2}{2m}\nabla^2\psi(\boldsymbol{r}) + V(\boldsymbol{r})\psi(\boldsymbol{r}) = E\psi(\boldsymbol{r}) \tag{1}$$

where $V(\boldsymbol{r})$ is an arbitrary potential.

If the potential $V(\boldsymbol{r})$ is spherically symmetric, that is $V(\boldsymbol{r}) = V(r)$, the problem can be simplified by supposing that the wave function can be written in the form

$$\psi(\vec{r}) = \frac{R_{n,l}(r)}{r} Y_{l,m}(\Omega_r) \tag{2}$$

where n, l and m are the quantum numbers necessary to fully define the state. As the angular component of the wave function does not depend on the potential $V(r)$ we are studying, we can focus only on the radial component. As a side note, the spherical symmetry leads to a degeneracy in the quantum number m.

If we introduce the function $u_{nl}(r) = R_{nl}(r)\, r$, we can rewrite the radial Schrödinger equation in the following form (the equation is called *reduced radial equation*):

$$\left[-\frac{\hbar^2}{2m}\frac{\partial^2}{\partial r^2} + V(r) + \frac{\hbar^2 l(l+1)}{2mr^2}\right] u_{n,l}(r) = E_{n,l}\, u_{n,l}(r) \tag{3}$$

We can identify two kinds of stationary states depending on the energy E of the system: bound states and free states. If the energy E is lower than the value of the potential at infinity $V(\infty)$ we have a bound state and the wave function goes to zero at infinity. Instead if E is higher than $V(\infty)$, we have a free (or scattering) state and the wave function does not go to zero at infinity, rather it oscillates. Moreover, bound states have a discrete energy spectrum while that of free states is continuous and the wave functions of the former must be normalised to have physical sense, while this is not necessary (and problematic from a mathematical point of view) for the latter.

When studying the bound states of a given potential, we are interested in the spectrum of the energy eigenvalues $E_{n\ell}$.

On the contrary, in a scattering experiment the attention is focused on some specific free states and the relevant physical quantities are the differential cross section $d\sigma(\Omega)/d\Omega$ and the total cross section $\sigma_{tot}(E)$. In what follows we shall obtain a numerical estimate for the latter in the aforementioned

scattering process.

For scattering states, if $V(r) \ll E$ $u(r)$ assumes the form:

$$u(r) \propto kr\left[(\cos(\delta_l) j_l(kr) - \sin(\delta_l) n_l(kr)\right] \tag{4}$$

where $k = \sqrt{2mE}/\hbar$ and j_l, n_l are the spherical Bessel and Neumann functions and δ_l is the *phase shift*, the set of which for all l fully defines the potential; in fact, the total cross section σ_{tot} can be obtained directly from the phase shifts as

$$\sigma_{tot} = \frac{4\pi}{k^2} \sum_{l=0}^{\infty} (2l+1) \sin^2 \delta_l \tag{5}$$

Considering eq. (4) one can find that the phase shifts δ_l can be calculated using the following formula:

$$\tan \delta_l = \frac{\kappa j_l(kr_2) - j_l(kr_1)}{\kappa n_l(kr_2) - n_l(kr_1)} \tag{6}$$

where

$$\kappa = \frac{u(r_1) r_2}{u(r_2) r_1} \tag{7}$$

and r_1 and r_2 are two points where the potential $V(r)$ is almost null.

We model the interaction between the Hydrogen and Krypton atoms with a simple Lennard-Jonnes potential

$$V_{LJ} = 4\varepsilon \left[\left(\frac{\sigma}{r}\right)^{12} - \left(\frac{\sigma}{r}\right)^{6} \right] \tag{8}$$

where, in principle, the parameters ε and σ should be fitted on the data of the experiment; in our case, we use $\varepsilon = 5.9\,\text{meV}$ and $\sigma = 3.18\,\text{Å}$. Physically σ represents the point where the Lennard-Jones potential is null, while $-\varepsilon$ is the minimum of the potential.

2 Introduction to the computation problem

To integrate the Shrödinger equation, we discretize the coordinate interval into a mesh $\{x_0, x_1, ..., x_{N-1}\}$ with $x_{i+1} - x_i = h$ and use the Numerov method. Given a generic 2^{nd} order homogeneous differential equation

$$\frac{d^2 y(x)}{dx^2} + k^2(x) y(x) = 0 \tag{9}$$

the algorithm calculates the function $y(x)$ at the $(i+1)$-th point of the mesh $y(x_{i+1}) = y_{i+1}$ starting from the two previous points y_i, y_{i-1} as

$$y_{i+1} = \frac{y_i \left(2 - \frac{5}{6} h^2 k_i^2\right) - y_{i-1} \left(1 + \frac{h^2}{12} k_{i-1}^2\right)}{1 + \frac{h^2}{12} k_{i+1}^2} \tag{10}$$

where $k_i = k(x_i)$. In our case, the equation, in the 1D case, is

$$\frac{\hbar^2}{2m} \frac{d^2 \psi_\alpha(x)}{dx^2} + (E_\alpha - V(x))\, \psi_\alpha(x) = 0 \tag{11}$$

where α is an appropriate set of quantum numbers. In the 3D case, if $V(\boldsymbol{r}) = V(r)$, the equation for the radial part $u_{n,l}(r)$ of the wavefunction $\psi_{n,l,m}(\boldsymbol{r}) = u_{n,l}(r) r^{-1} Y_{l,m}(\Omega_r)$ has the same form of eq. (11) with an effective potential

$$V_{\text{eff}}(r) = V(r) + \frac{\hbar^2}{2m} \frac{l(l+1)}{r^2}$$

and so, in the Numerov algorithm, we have

$$k^2(r) = \frac{2m}{\hbar^2}\left[E_{n,l} - V(r) - \frac{\hbar^2}{2m}\frac{l(l+1)}{r^2}\right] \tag{12}$$

We implemented the code in the following way:

```
// Algorithm that implements Numerov and propagates the wave function,
// starting from the center
void Numerov(int N, int l, double E, double h, double* y, double (*V) (double))
{
  double h2=h*h;

  // Calculate k^2
  double* k2 = new double[N+1]; // k^2 array
  for(int i = 1; i < N+1; i++)
  {
    k2[i] = 2*(E - V(i*h)) - l * (l +1.0) / (i*i*h2);
  }

  // Initial conditions
  y[0] = 0.;
  y[1] = pow(h, l+1);
  y[2] = pow(2*h, l+1);

  // Apply Numerov Algorithm
  for(int i = 2; i < N; i++)
    {
      y[i+1] = (y[i]*(2.0 - 5.0/6.0 * h2 * k2[i]) - y[i-1]*(1.0 + h2 /12.0* k2[i-1]))
      ... / (1.0 + h2 / 12.0 * k2[i+1]);
    }
  delete[] k2;
}
```

If one wanted to, say, use Numerov's algorithm to find the bound states with their respective energies of a potential of which the analytical solutions are not available, it can be noticed e.g. from eq. (10) and eq. (12) that the Numerov step requires the energy of the state. As this is not available, one could exploit the fact that, at least from a theoretical standpoint, only the correct energy gives a wavefunction which goes to 0 as the coordinate x goes to ∞. For this reason, if one assumes that $y(x = \infty, E)$ is a continuous function of the value of E used in Numerov, one could use a root-finding algorithm to solve $y(x = \infty, E) = 0$ and get the correct energy eigenvalue and thereby also the bound state wavefunction. Clearly, it is not possible to calculate $y(x = \infty)$ and so one may choose an appropriate $x_{\max}$ and then solve $y(x_{\max}, E) = 0$[1]. Of course, this is an approximation, and so it is useful to repeat the same process for different values of $x_{\max}$ to assess whether the approximation is affected by it. In what follows we shall use the false position method as root-finding algorithm. Given $y(x_{\max}, E_1)$ and $y(x_{\max}, E_2)$ such that $y(x_{\max}, E_1)y(x_{\max}, E_2) < 0$, we calculate a new approximation E_{new} of the energy E_0 for which $y(x_{\max}, E_0) = 0$ as

$$E_{\text{new}} = E_1 - y(x_{\max}, E_1)\frac{E_1 - E_2}{y(x_{\max}, E_1) - y(x_{\max}, E_2)} \tag{13}$$

We then either set $E_1 = E_{\text{new}}$ or $E_2 = E_{\text{new}}$ based on where $y(x_{\max}, E)$ changes sign and iterate the process until the energy values at a certain iteration are equal up to a fixed threshold E_t[2]. We prefer this algorithm over the secant method because it is guaranteed to converge whereas the latter is not. A way

[1] It is clear that in this case $y(x_{\max}) \neq 0$; rather, the correct energy is the one for which $y(x_{\max})$ *differs from 0 the least*, and the procedure we employ allows to find such value.

[2] It is more convenient to impose a threshold on E rather then on $y(x_{\max}, E)$ even when $y(x)$ is normalized, as this should be adapted based on $r_{\max}$ in a non-trivial way to allow a comparison between the results.

to implement the false position method could be the following:

```
// Loop for false position method
    while(j < MaxCycles && abs(E2 - E1) > Et)
    {
      // Formula to calculate next energy we will use
      Eaux = E1 - y1 * (E2 - E1) / (y2 - y1);
      // I use Numerov
      Prop(N, l, Eaux, h, y, V);

      // Condition for choosing the next point

      // When both the point have the same sign
      if(y[N]*y1 > 0)
      {
        y1 = y[N];
        E1 = Eaux;
      }
      // When the point have different sign
      else if(y[N]*y1 < 0)
      {
        y2 = y[N];
        E2 = Eaux;
      }
      // When the algorithm gives the zero
      else if(y[N]*y1 == 0)
      {
        E2 = Eaux;
        E1 = E2;
      }
      j++;
    }
```

As shown in eq. (6), to calculate the phase shifts we need to evaluate the spherical Bessel and Neumann functions of order l $j_l(x)$ and $n_l(x)$ for an arbitrary argument. There exists an easy and fast iterative procedure to do so, namely if we define

$$\begin{aligned} j_{-1}(x) &= \frac{\cos x}{x} \quad j_0(x) = \frac{\sin x}{x} \\ n_{-1}(x) &= \frac{\sin x}{x} \quad n_0(x) = -\frac{\cos x}{x} \end{aligned} \tag{14}$$

we call $s = j, n$ we have

$$s_{l+1}(x) = \frac{2l+1}{x} s_l(x) - s_{l-1}(x) \tag{15}$$

3 Discussion

Before actually considering the scattering problem, we may want to check the correctness of the code as well as the characteristics of the Numerov algorithm. To do this, we consider an Hamiltonian of which the eigenvalues and eigenfunctions are known analytically, that is the harmonic oscillator (HO). We first consider the 1D case then switch to the 3D one, which is more closely related to the original scattering problem we shall deal hereafter.

3.1 Point 1

The 1D HO Hamiltonian (written in some arbitrary units) is given by

$$H_{HO} = -\frac{1}{2}\frac{\partial^2}{\partial x^2} + \frac{1}{2}x^2 \tag{16}$$

and has eigenvalues

$$E_n = n + \frac{1}{2}$$

where $n = 0, 1, ...$ is the only quantum number needed to fully characterize the states; the corresponding eigenfunctions are

$$\psi_n(x) = \frac{1}{\sqrt{2^n n!}}\pi^{-1/4} H_n(x) e^{-x^2/2}$$

where $H_n(x)$ is the Hermite polynomial of order n.

As seen in the previous section, to start with the numerical integration the Numerov algorithm requires the values of the wavefunction calculated in the first two points of the mesh. As the potential goes to infinity at $|x| \to \infty$, we expect the wavefunctions to go to zero in the same limit, therefore we could make an approximation and set $y_0 = 0$ at some x_0 suitably chosen, e.g. some multiple of the classical inversion point, where $E = V(x)$ (we shall address the question of the energy in a moment). We could then set y_1 to an arbitrary value to then fix it imposing the correct normalization. However, we can also make a more convenient choice and exploit the symmetries of the Hamiltonian; in fact, from eq. (16) we can see that the eigenfunctions of the 1D HO are either even or odd. Additionally, in the odd case at $x \to 0$ at first order in x the potential is null and so the eigenfunctions are sine waves, so we can choose $y_0 = 0$, $y_1 = h$. A for the even case, calling $y_n = y(0)$, we have $y_{n+1} = y_{n-1}$, and so we can rewrite the Numerov algorithm as

$$y_1 = \frac{y_0}{2}\frac{\left(2 - \frac{5}{6}h^2k_0^2\right)}{\left(1 + \frac{1}{12}h^2k_1^2\right)}$$

where we have also used the fact that also the potential is even. We can then integrate the wave function using the algorithm and then mirror the result with respect to the origin or the y axis respectively. This way we can halve the computational time as well as decrease the number of integration points and so accumulate less error.

We can first check the correctness of the calculated eigenfunctions. Below we compare the first five wave functions obtained with the Numerov algorithm with the analytical ones:

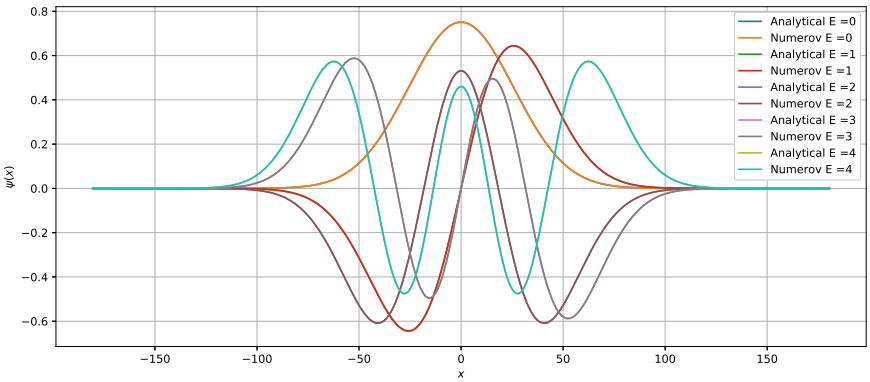

Figure 1: Comparison between wave functions obtained with the analytical formula and the Numerov algorithm($h = 0.00151, r_{max} = 7$). As we can see, the functions from Numerov are perfectly overlapped to the analytical ones.

As we can see from fig. 1, the calculated wave functions show the same behaviour of the analytic ones.

We can also perform a quantitative check on the calculated wave functions and on how they change as of the number of mesh points we use changes. If the wave function is identical to the analytic solution (and properly normalized), we expect the modulus of their scalar product to be 1:

$$|\langle\psi_{anal}|\psi_{Numerov}\rangle|^2 = 1 \tag{17}$$

It is important to notice that *both* functions need to be normalized and not only the one that we calculate using Numerov. The reason is that we calculate the scalar product only on a small region ($[-r_{\max}, r_{\max}]$); if we neglected this, the maximum value of the scalar product would not be 1 anymore.

It makes sense to define the error on the wave function ϵ in the following way:

$$\varepsilon = 1 - |\langle\psi_{anal}|\psi_{Numerov}\rangle|^2 \tag{18}$$

We run the algorithm for different values of mesh steps h and different energies. The results are portrayed in fig. 2.

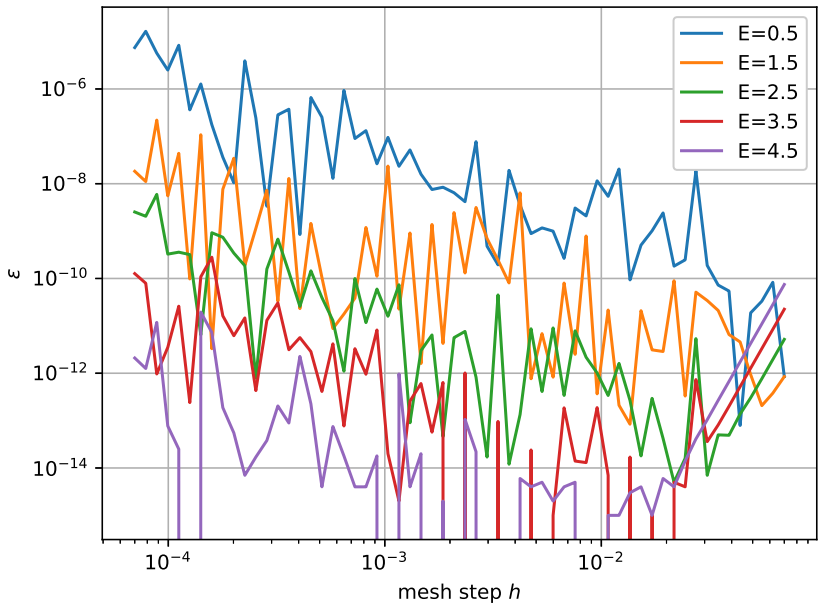

Figure 2: Plot of the error ε on the wave functions as a function of the mesh step h for different values of the energy, in logarithmic axis.

We can immediately notice from fig. 2 that the error seems to decrease as h increases up to $h = 0.01$ (in general the error for $h \simeq 0.01$ is smaller of 2-4 orders of magnitude than that at the smallest h). After $h = 0.01$ the error seems to increase with a power law[3] (we clearly see straight lines for $E = 3.5, 4.5$). Despite the error seems to have a power law trend, we can see that the error oscillates wildly for small variations of h (the oscillations cover several orders of magnitude). This suggests us that checking the error on the eigenfunctions to evaluate the precision of the Numerov algorithm is not a good idea, because the error changes a lot for similar values of h and it is difficult to find an optimal value. Lastly, we shall see that if the value of h which minimizes the error on the wave function yields a rather big minimum error on the energies (some are are of the order of 10^{-6}, while for other h we get much lower errors). So

[3]It is important to remember that a power law behaviour will appear as a linear behaviour in a loglog plot.

it seems that having a small error on the wave function does not translate in a small error on the energy E.

Moreover, we can see that the algorithm seems to behave better when calculating wave functions corresponding to higher energies. This may be due to the fact that the algorithm start to diverge when we pass other the classical inversion point and the higher energy, the farther away this point is. We think that the reason why the algorithm diverges is due to the fact that the possible solutions for the SE at one extremity are two exponentials, one with positive exponent and one with negative exponent. The computer does not know which the physical solution is and picks a sum of the two, therefore we get something that, at some point, diverges. Another interesting fact is that the higher the energy, the earlier the error starts to increase again for high h.

Finally, looking at fig. 2, we can see that we miss some values of ϵ for some h. This can be explained by the fact that when we compare the analytical function and the one that we get from Numerov, we have to normalize both functions. When we do this, we introduce an error due to the integration algorithm (in our case the Cavalieri-Simpson method). We have estimated that the error on the norm of our wave functions is of the order of $10^{-14} - 10^{-16}$, therefore sometimes we get that the scalar product is slightly higher than 1 and we get a negative ϵ (that we cannot plot in a loglog plot).

From this brief analysis we can see that looking at the wave function to evaluate the optimal value of h is not a good method. Thus it make sense to study the values of energies E that we get instead, because it may be a more stable method. Before analysing the error on the energies, one could wonder why we did not check the precision of the Numerov algorithm using the correct analytic energies, instead of using the one that we get from the false position method. At first it could seem that Numerov would yield a more accurate result by proceeding in this way (and we could estimate separately the errors due to the propagation of the wave function and the error due to the false position method), but this is false. In fact if we apply Numerov with the analytical energies the wave function diverges earlier, as we can see for example in fig. 3. This is due to the fact that the false position method determines the energy that minimise the divergence of the wave function and this value does not always correspond to the analytic value of E.

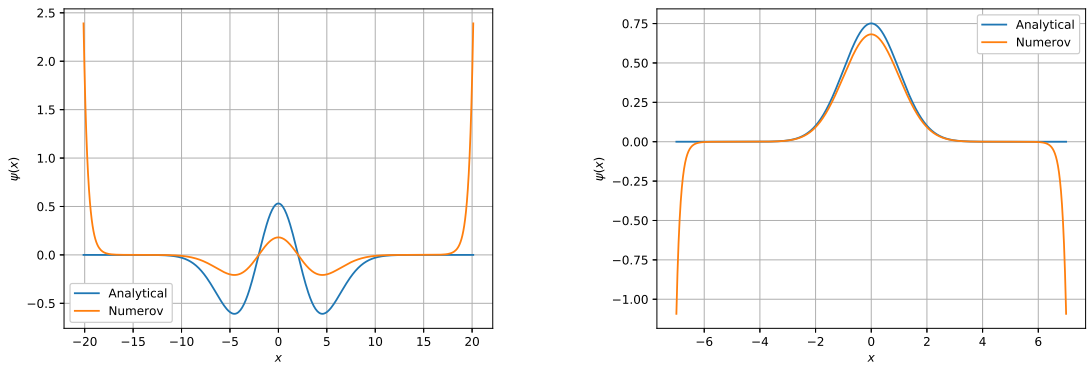

Figure 3: Comparison between wave functions obtained with the analytical formula and the Numerov algorithm using the analytical energies. On the left we have used $E = 2.5, h = 0.033$ and on the right we have used $E = 0.5, h = 7 \times 10^{-5}$.

To check the correctness of the energy eigenvalues and the dependence of the solutions on the points of the mesh, we initially tested the algorithm using 20 different mesh steps and 4 different final positions $x_{\max}$. As we can notice in fig. 4 and fig. 5, as the energy threshold is lowered all curves follow the same behaviour independently on $x_{\max}$ (at least for low n - we shall discuss this in a moment) and only display fluctuations on the order of the threshold imposed.

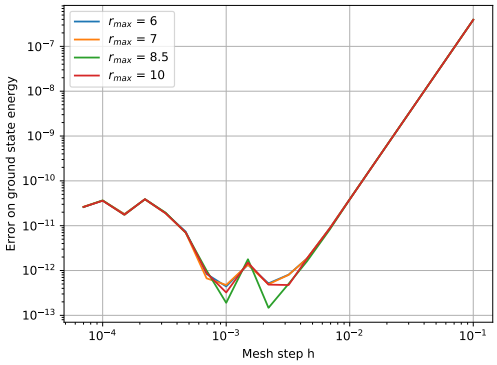

Figure 4: Error on ground state energy for a threshold $E_t = 10^{-12}$ for different values of $x_{\max}$. Notice the fact that the curves only differ on the order of the threshold.

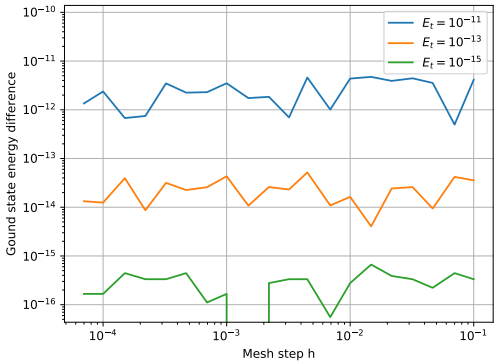

Figure 5: Difference between numerical values of the ground state energy using $x_{\max} = 10$ and $x_{\max} = 8.5$ for different thresholds.

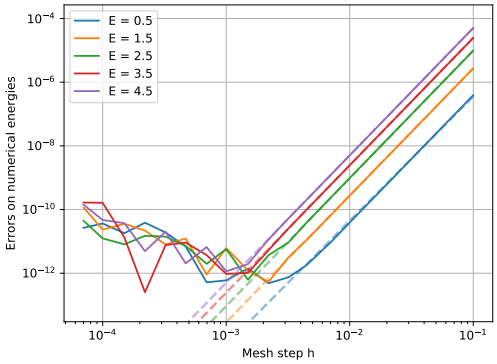

Figure 6: Errors for the first 5 energy eigenvalues with suitably chosen $x_{\max}$ (10) and E_t (10^{-13}). The plot also shows fits for the highest values of h.

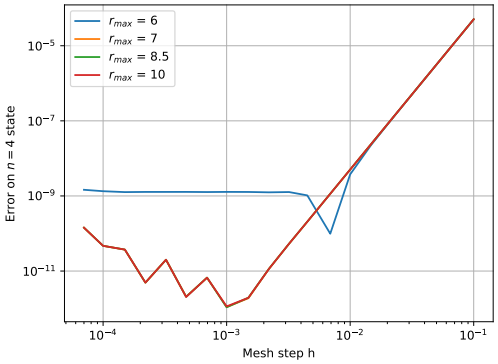

Figure 7: Effect of using $x_{\max} = 6$ on the error of $E = 4.5$, too small to contain all the relevant fluctuations of the wave function.

Clearly, the results do no depend over $x_{\max}$ as long as this value is big enough to well contain all the relevant fluctuations of the wavefunction, which for some of the tested values is not the case for the highest values of n considered (See fig. 7). Therefore, considering a suitable $x_{\max}$ and using a threshold low enough not to influence significantly the behaviour of the errors, we can identify a common behaviour in all the error curves: a power law behaviour for the highest values of h, then the errors reach a minimum and then increase again. We performed a fit on the power law part of the curves, the results are presented in table 1 and shown in fig. 6.

Energy	Slope
0.5	3.9806
1.5	4.0058
2.5	4.0028
3.5	4.0009
4.5	4.0011

Table 1: Fitted parameters for the error against the 9 largest values of h for the first 5 energies.

We can observe that the dependence is close to h^4, as the Numerov algorithm itself. This is reasonable,

since the global error of the method is $\mathcal{O}(h^4)$ and we use the value of the wavefunction at $x_{\max}$ in the root-finding algorithm.

As mentioned above, at small enough h the errors reach a minimum and change behaviour. It is thus interesting to check more in detail this interval of h. fig. 8 pictures the error on the ground state, the 2^{nd} excited state and the 4^{th} excited state, imposing $E_t = 10^{-15}$ and choosing $r_{\max} = 10$ (this doesn't really influence the result as discussed above) for 100 values of h around the minimum.

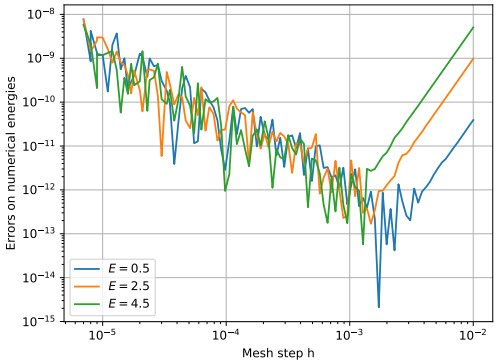

Figure 8: Zoom on the minimum of the error for $E = 0.5$, 2.5 and 4.5 using $x_{\max} = 10$ and $E_t = 10^{-15}$.

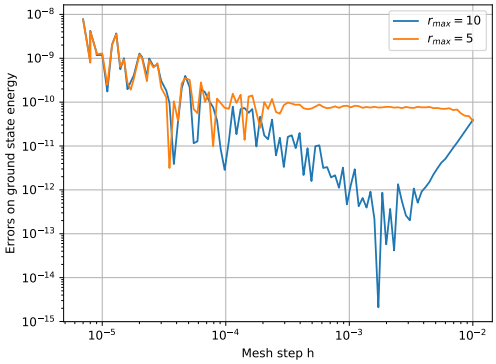

Figure 9: Zoom on the effect of using $x_{\max} = 5$ for the error on the ground state ($E_t = 10^{-15}$).

The fact that the curves at high h do not overlap may be due both to the fact that we use the same threshold and the same $x_{\max}$ for all energies. It is interesting, however, that all curves show a power law behaviour which depends solely on h.

We can identify three kinds of errors: the error due to the Taylor expansion in the Numerov algorithm, the error due to the loss of numerical precision and the error due to a bad choice of x_{max}. The first is dominant at high h; on the contrary, the second, when significant, imposes a constant lower bound to the error. The error due to the loss of numerical precision is dominant at small h instead.

3.2 Point 2

Before moving on to the scattering problem, we can consider another problem of which the analytical solution is known but which is more closely related to the one we're about to study: the 3D harmonic oscillator. In some arbitrary units, its Hamiltonian is given by

$$H_{HO} = -\frac{1}{2}\frac{\partial^2}{\partial r^2} + \frac{1}{2}r^2 + \frac{l(l+1)}{r^2} \tag{19}$$

and the eigenvalues are

$$E_n = 2n + l + \frac{3}{2}$$

where $n = 0, 1, \ldots$ is the principal quantum number and l is the angular momentum; the corresponding eigenfunctions are

$$\psi_{n,l,m}(r) = N_{n,l}\, r^l L_n^{(l+1/2)}(r^2) e^{-r^2/2} Y_{l,m}(\Omega_r)$$

where $L_n^{(l+1)}(r)$ is a generalized Laguerre polynomial and

$$N_{n,l} = \sqrt{\sqrt{\frac{1}{4\pi}} \frac{2^{n+l+3} n!}{(2n+2l+1)!!}}$$

is a normalization factor.

In this case we can actually perform the same analysis as in the previous point. However, as the effective potential diverges for $r \to 0$ (in the $l > 0$ case), we need to use suitable initial conditions and it is convenient to start from an initial coordinate $r_0 = h$. One can prove that, as $r \to 0$, the radial wave function $u_{n,l}(r)$ goes like r^{l+1}, and so we can choose $\left(h,\, h^{l+1}\right)$, $\left(2h,\, (2h)^{l+1}\right)$ as the two initial points for the Numerov algorithm. In fig. 10, fig. 11 and fig. 12 we present the results for the energy errors, already with a large enough $r_{\max}$ and a small enough E_t.

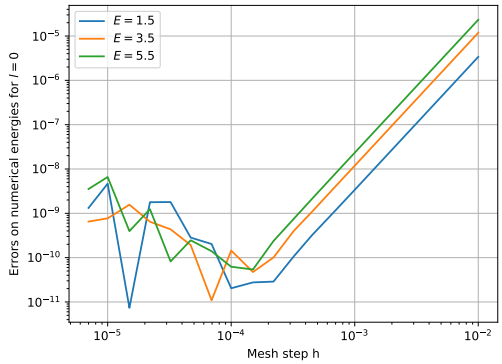

Figure 10: Error on states with $l = 0$ considering $E_t = 10^{-13}$ and $r_{\max} = 10$.

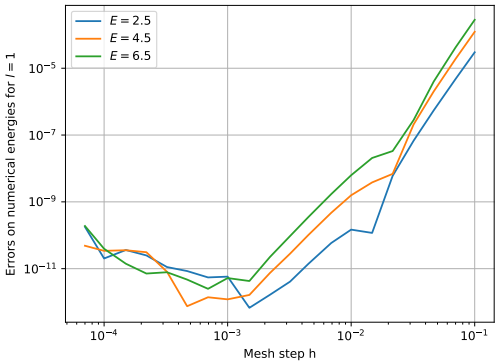

Figure 11: Error on states with $l = 1$ considering $E_t = 10^{-13}$ and $r_{\max} = 10$.

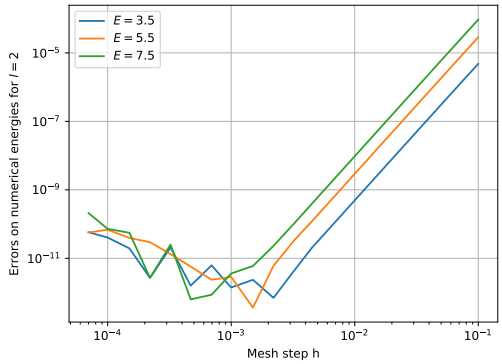

Figure 12: Error on states with $l = 2$ considering $E_t = 10^{-13}$ and $r_{\max} = 10$.

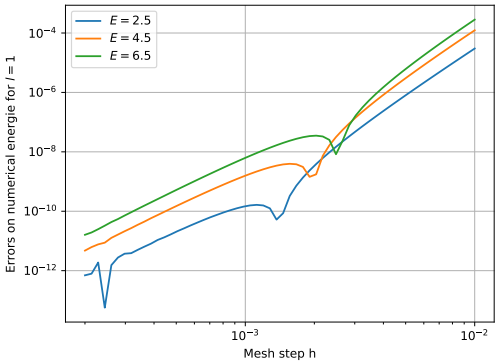

Figure 13: Zoom on error on states with $l = 1$, $E_t = 10^{-13}$ and $r_{\max} = 10$.

Contrarily to the 1D case, these plots show discordant behaviours for the first values of h. In particular, the case $l = 0$ (fig. 10) shows a dependence on h^3 rather than on h^4 (we performed fits in the first part of the graphs to assess this behaviour). It is interesting to notice that the SE for the 3D HO in the $l = 0$ case is actually the same as that for the 1D case, which we already discussed above (clearly, only the odd states need to be considered to fulfill the request $u_{n,0} \to 0$ as $r \to 0$). In the previous section we actually obtained a h^4 dependence in these states, but the integration started from $x = 0$ rather than $r = h$. We can therefore attribute this discrepancy to the initialization of the wave function. A pathological behaviour is also shown by the $l = 1$ case (fig. 13), where the errors have a dependence of h^α where $\alpha \geq 5$ for big h, show a local minimum depend on the energy eigenvalue, then follow the expected h^4 behaviour. The case $l = 2$ show no unexpected behaviours. These issues could be explained by the fact that, the smaller the l, the more the behaviour at $r \to 0$ is important in the evolution of the wave function, though we choose not to investigate any further. On the contrary, for low h the error due to numerical precision

is dominant for all values of l as in the 1D case (see fig. 14).

In fig. 15 are shown the obtained wavefunctions for the 3D HO, using the optimal parameters discussed above.

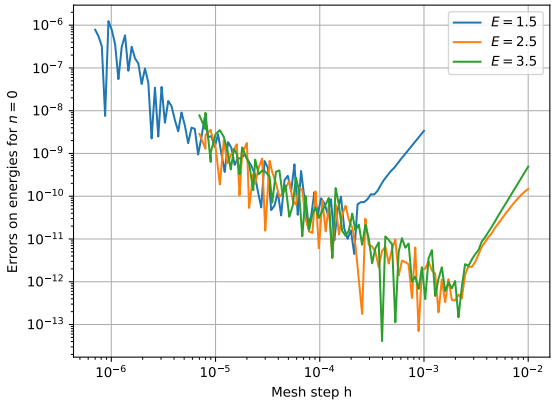

Figure 14: Zoom on errors of the energy eigenvalues for $n = 0$ around the minimum.

3.3 Point 3

As said in section 2, the spherical Bessel functions can be easily evaluated using eq. (15). We have implemented the iterative method as follows:

```
//Function for evaluating Bessel j_l functions
double bessel_j(double x, int l)
{
    double j_1,j0,j1;

    //Initial conditions fixed by the first two analytical bessel functions
    j_1=cos(x)/x;
    j0=sin(x)/x;

    if(l>0)
    {
        for(int i=0;i<l;i++)
        {
            // Recursive formula for Bessel functions
            j1=(2*i+1)/x*j0-j_1;
            j_1=j0;
            j0=j1;
        }
    }
    return j0;
}
```

The code for the Neumann functions is identical except for the initial conditions.

The spherical functions for $l = 1, 2, 3$ are shown in fig. 16.

We can test the correctness and the precision of this method by comparing our result with the

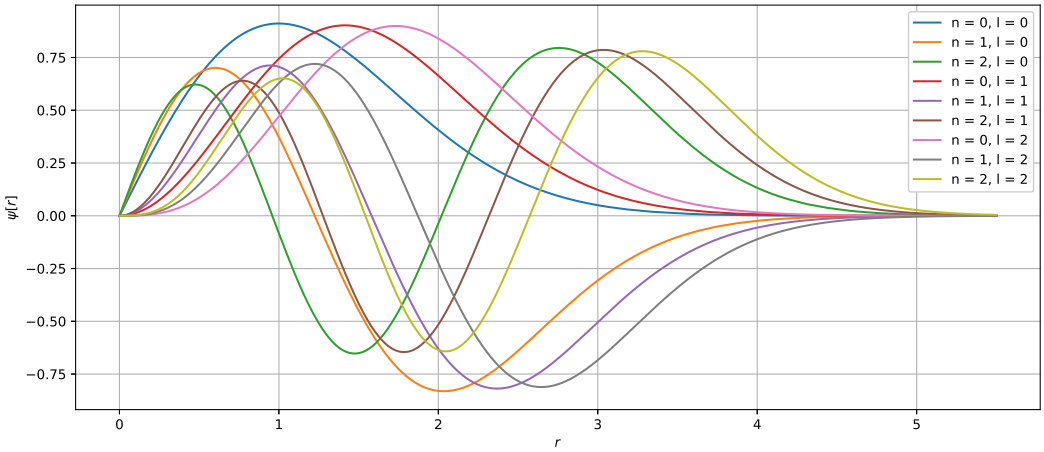

Figure 15: Wave functions of the 3D HO that we obtained from Numerov.

analytical form of the functions:

$$j_1(x) = \frac{\sin x}{x^2} - \frac{\cos x}{x} \quad j_2(x) = \left(\frac{3}{x^2} - 1\right)\frac{\sin x}{x} - \frac{3\cos x}{x^2} \quad j_3(x) = \left(\frac{15}{x^3} - \frac{6}{x}\right)\frac{\sin x}{x} - \left(\frac{15}{x^2} - 1\right)\frac{\cos x}{x}$$

$$n_1(x) = -\frac{\cos x}{x^2} - \frac{\sin x}{x} \quad n_2(x) = \left(-\frac{3}{x^2} + 1\right)\frac{\cos x}{x} - \frac{3\sin x}{x^2} \quad n_3(x) = \left(-\frac{15}{x^3} + \frac{6}{x}\right)\frac{\cos x}{x} - \left(\frac{15}{x^2} - 1\right)\frac{\sin x}{x}$$

The behaviour of the absolute error of our functions is shown in fig. 17. We can see that, for low values of x, the error is bigger for higher values of l; moreover we see that the Neumann functions (which diverge for $x \to 0$) have an error which is comparable to the one of the Bessel of the successive order. However we need to evaluate the Bessel functions for big values of x (namely $x > 4$) and in that area all the errors are of order 10^{-16}. This error is way smaller than any other error our code is working with, so it is not a problem.

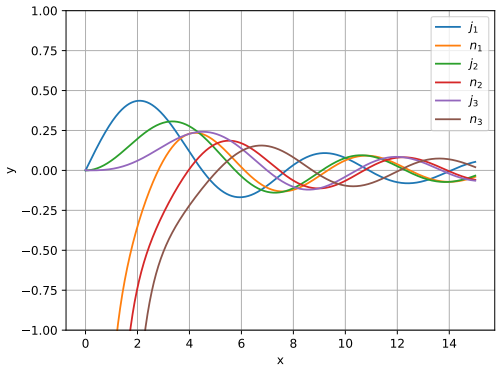

Figure 16: Plot of the Bessel functions calculated using the recursive formula for $l = 1, 2, 3$.

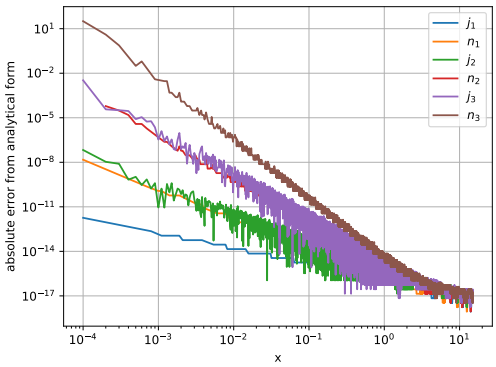

Figure 17: Absolute value of the error of the Bessel functions evaluated using the recusion formula from the analytical ones for $l = 1, 2, 3$.

3.4 Point 4

When performing numerical calculations, it is often wise to use suitable measurement units in order to deal with quantities close to unit and avoid inconsistent results due to a computer's internal representation of floating point numbers. The Lennard-Jones potential is defined by two parameters, ϵ and σ, that set the scales of energy and length of the problem. Moreover, the interaction potential only affects the relative motion of the two atoms, therefore we can choose to work in the center of momentum frame and use the relative mass as reference mass:

$$\mu = \frac{m_{\mathrm{H}} m_{\mathrm{Kr}}}{m_{\mathrm{H}} + m_{\mathrm{Kr}}} = 1.6536 \times 10^{-27}\mathrm{Kg} \tag{20}$$

Thus we can rewrite every quantity of the problem in units of these three reference parameters: ϵ, σ and μ. Clearly the physical constants will assume different values; in particular $\hbar$ will be rewritten in the following way:

$$\hbar = \hbar' \mu^{\alpha} \sigma^{\beta} \epsilon^{\gamma} \tag{21}$$

where $\hbar'$ is the reduced Planck constant in the new measurement units and α, β, γ are suitable exponents. To obtain the three exponents, we perform a dimensional check on the previous equation:

$$[\hbar] = \mathrm{m}^2 \mathrm{Kg}\, \mathrm{s}^{-1}$$
$$[\mu^{\alpha} \sigma^{\beta} \epsilon^{\gamma}] = \mathrm{m}^{2\gamma+\beta} \mathrm{Kg}^{\alpha+\gamma} \mathrm{s}^{-2\gamma}$$

If we equate the exponents of the two previous equations we get:

$$\alpha = \frac{1}{2}\ , \quad \beta = 1\ , \quad \gamma = \frac{1}{2}$$

Thus the reduced Planck constant becomes:

$$\hbar' = \frac{\hbar}{\sigma\sqrt{\mu\epsilon}} = 0.26524240934$$

In the next section, we shall drop the primes and only refer to the quantities in these new units for ease of notation.

3.5 Point 5

Switching now our attention on the scattering problem with the Lennard-Jones potential, as we did for the other potentials we shall first consider the issue of the inizialization of the wave function. In this case it can be found that, in the limit $r \to 0$, the wave function assumes the form:

$$\lim_{r\to 0} \psi(r) = A\, e^{-\left(\frac{b}{r}\right)^5} \tag{22}$$

where A is the normalization constant and b is a parameter that depends on the other relevant quantities of the problem, i.e. μ, ϵ and σ. Note that in this limit the wave function do not depend on the value of l.

To obtain b, we can plug Eq. (8) and Eq. (22) into Eq. (3):

$$\left[-\frac{\hbar^2}{2}\frac{\partial^2}{\partial r^2} + 4\left[\left(\frac{1}{r}\right)^{12} - \left(\frac{1}{r}\right)^{6}\right] + \frac{\hbar^2 l(l+1)}{2r^2}\right] A\, e^{-\left(\frac{b}{r}\right)^5} = EA\, e^{-\left(\frac{b}{r}\right)^5} \tag{23}$$

In the limit $r \to 0$ we can keep only the higher orders of r^{-1} and so we get

$$\frac{\hbar^2}{2}\frac{\partial^2}{\partial r^2}\left[e^{-\left(\frac{b}{r}\right)^5}\right] = 4\left(\frac{1}{r}\right)^{12} e^{-\left(\frac{b}{r}\right)^5} \tag{24}$$

The second derivative of the exponential is

$$\frac{\partial^2}{\partial r^2}\left[e^{-\left(\frac{b}{r}\right)^5}\right] = \left(\frac{25\,b^{10}}{r^{12}} - \frac{30\,b^5}{r^7}\right) e^{-\left(\frac{b}{r}\right)^5} \quad \to \quad \frac{25\,b^{10}}{r^{12}} e^{-\left(\frac{b}{r}\right)^5} \text{ for } r \to 0 \tag{25}$$

Therefore we finally get

$$\frac{\hbar^2}{2}\frac{25\,b^{10}}{r^{12}} e^{-\left(\frac{b}{r}\right)^5} = 4\left(\frac{1}{r}\right)^{12} e^{-\left(\frac{b}{r}\right)^5} \quad \Rightarrow \quad b^5 = \sqrt{\frac{8}{25\hbar^2}} = 2.13271107873 \tag{26}$$

This means that for small r the wavefunction is very small (i.e. $\log(\psi(r = 0.2)) \sim -10^5$). Dealing with such small numbers poses a problem from the computational point of view, since a normal computer treats them as zero. To solve this issue we could easily modify the Numerov algorithm in Eq. (10) such that it only contains *the logarithm* of the function. Nevertheless, we don't discuss this procedure further since, for our purposes, it shall prove to not be necessary.

3.6 Point 6

In order to solve the scattering problem we need to modify the Numerov algorithm tested with the harmonic oscillators. First of all we are no longer searching for bound states and their energy, so the root finding algorithm is no longer necessary. Moreover, as discussed in section 3.4, it is better to use σ, ε and μ as fundamental units and therefore $\hbar$ cannot be set to 1 anymore[4]. Finally, since we are not dealing with bound states, the initial conditions have to be taken as shown in section 3.5. However, as mentioned above, there may be a computational problem due to the fact that the wave function close to the origin is very small and a standard computer may approximate it to zero (of course we have to exclude a priori the point $r = 0$ to avoid division by zero problems).

In a scattering problem we are interested in calculating the total cross section, that we can obtain using eq. (5) and eq. (6). In this section we analyze how the computed phase shifts from eq. (6) depend on the choice of the initial condition and of the points r_1, r_2. In order to do so we fix the energy $E = 0.3\,\varepsilon$, the maximum angular momentum quantum number $l = 6$ and the final value of r in the mesh $r_{fin} = 15\,\sigma$. We have chosen r_{fin} large enough for the potential to be zero in a good approximation (the potential is already close to zero at $r = 5\,\sigma$), but not too big to affect the execution time of the program. We set $h = 0.001$ because, even if the situations are different, in section 3.2 we obtained that for this mesh step we had the smallest energy error.

Now we shall discuss the variation of the phase shifts as function of the parameters r_{min}, r_{max}, r_{gap}, which are respectively the starting point where we set the initial condition for Numerov algorithm, the point r_1 that we use in eq. (6) and the distance between r_1 and r_2. When we are analyze the dependence of the phase shift on one of the three parameters, the other two will be set to fixed values (later we shall explain the reason why we choose these values in particular): $r_{min} = 0.4\,\sigma$, $r_{max} = 11\,\sigma$, $r_{gap} = 0.5\,\sigma$.

We start by looking for the lowest possible value of r_{min} for which $\exp\left(-b^5/r_{min}^5\right)$ is not approximated to zero by the computer. After some trials we got that r_{min} must be higher of $0.31\,\sigma$. In fig. 18 it is shown how the phase shifts depend on r_{min}, for $r_{min} \in [0.31\,\sigma, 1\,\sigma]$. We see that the results are constant up to $r_{min} \simeq 0.8\,\sigma$. We can see better this trend in fig. 19, where we plotted the difference between the phase shifts evaluated at $r_{min} = 0.31\,\sigma$ and at an arbitrary $r_{min} \in [0.31\,\sigma, 1\,\sigma]$. We see that the difference

[4]It is important to modify accordingly the term $k^2(r)$ in the Numerov algorithm.

oscillates around a constant value until $r_{min} \leq 0.7\,\sigma$. This is probably due to some computational error. After $r_{min} = 0.7\,\sigma$ the error increases of several order of magnitude. We chose $r_{min} = 0.4\,\sigma$ as the starting point of the Numerov algorithm, because the phase shifts that we obtained are not influenced by this choice, but at the same time we avoid the possible instability of the point close to $r_{min} = 0.31\,\sigma$.

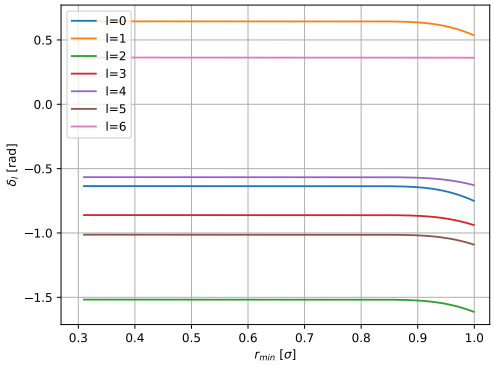

Figure 18: Plot of the phase shifts as functions of the starting point where we set initial conditions $r_{min} \in [0.31\,\sigma, 1\,\sigma]$.

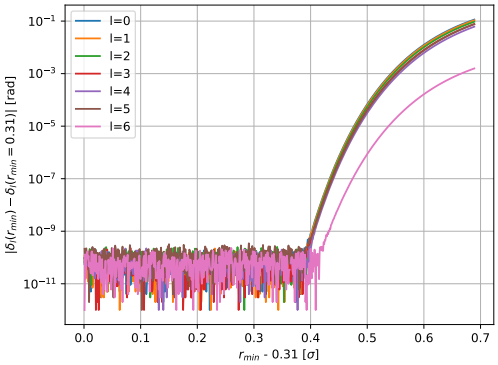

Figure 19: Absolute value of the difference between the phase shifts evaluated with starting point $r_{min} = 0.31\,\sigma$ and $r_{min} \in [0.31\,\sigma, 1\,\sigma]$.

We now analyse how the phase shifts are influenced by $r_1 = r_{max}$. We have calculated $\delta_l(r_{max})$ for several r_{max} and we have plotted the results in fig. 20; it seems that all the phase shifts are constant. However if we look at the relative variation $\delta_l(r_{max})/\delta_l(r_{max} = 14.4\,\sigma)$ (fig. 21), we see that this is not true. We chose to calculate the relative variation with respect to the largest value of r_{max}, because the potential is almost null. We can see that the relative variations are at most of order 0.8%, but chooisng $r_{max} > 10\,\sigma$ reduces drastically the variation. We think that $r_{max} = 11\,\sigma$ is a good balance between precision and execution time.

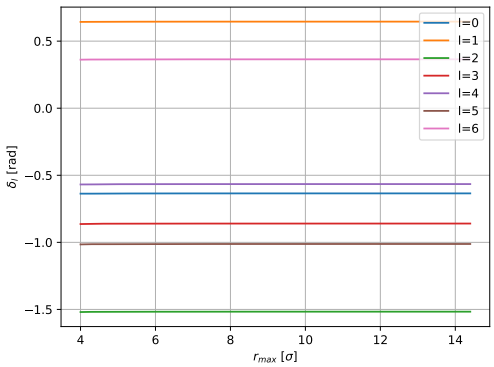

Figure 20: Plot of the phase shifts as functions of the position of $r_{max} \in [4\,\sigma, 14.4\,\sigma]$.

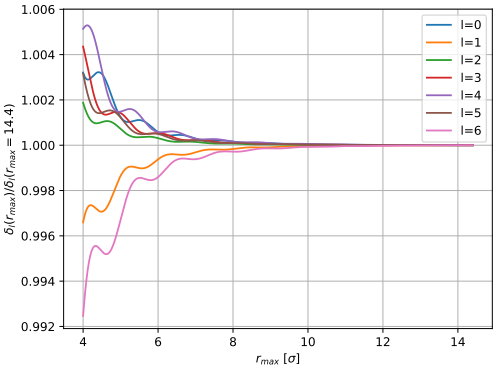

Figure 21: Relative variation of the phase shifts evaluated with respect to the largest point $r_{max} = 14.4\,\sigma$ and $r_{max} \in [4\,\sigma, 14.4\,\sigma]$.

Lastly we study the dependence of the phase shifts with respect to the distance between the points r_1, r_2, r_{gap}. In fig. 22 we can see that the phase shifts apparently do not depend on the distance between the two points, at least inside the interval $r_{gap} \in [0.1\,\sigma, 3\,\sigma]$. We proceed as before by defining the relative variation of the phase shifts with respect to $\delta_l(r_{gap} = 3\,\sigma)$. The results are in fig. 23. We observe that the relative variations is in general really small, of the order of 10^{-5}, except for some high peaks concentrated around a defined value of r_{gap}. These are a consequence of how we evaluate the phase shifts. We can see

this by substituting a sine function for the wave function in eq. (7), with the terms r_1 and r_2 that differ of a small value ϵ. ϵ in our case corresponds to a small difference of the Lennard-Jones potential between r_1 and r_2. What we get is:

$$\kappa = \frac{\sin(r_1)r_2}{\sin(r_2+\epsilon)r_1}$$

The result is shown in fig. 24. We can see that the peak in $x_{peak} = \pi$ has the same shape of the peaks in figure fig. 25. This means that the peaks are found at $r_{peaks} = n\frac{\lambda}{2}$, where λ, in our problem, is an approximate wavelength of the wavefunction for high enough r. We can the write

$$r_{peak} = \frac{\lambda}{2} = \frac{\pi}{k} \simeq \frac{\pi}{\sqrt{E - \frac{l(l+1)}{r_{max}^2}}} \simeq \frac{\pi}{\sqrt{E}}\left(1 + \frac{l(l+1)}{2\,r_{max}^2}\right)$$

where we have approximated the values of k and r_{max} to be equal for both r_1 and r_2 and we have ignored the Lennard-Jones potential, as it's negligible with respect to the centrifugal one. The previous formula shows that the position of the peaks depends on l and have a quadratic behaviour. In fact, fig. 25 shows a zoom on the first group of peaks and we can see that they behave exactly as predicted. Thus every value in the investigated interval is good, except when r_{gap} is equal to r_{peak}. We choose to use $r_{gap} = 0.5\,\sigma$.

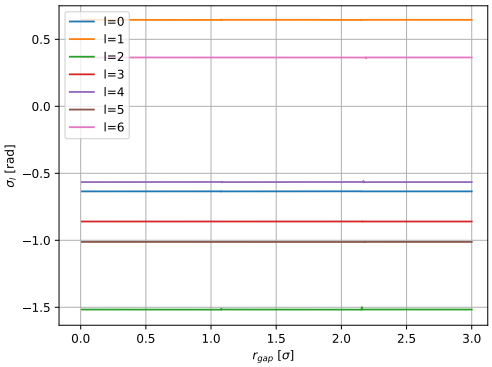

Figure 22: Plot of the phase shifts as functions of the distance between the two points $r_2 - r_1 = r_{gap} \in [0.1\,\sigma, 3\,\sigma]$.

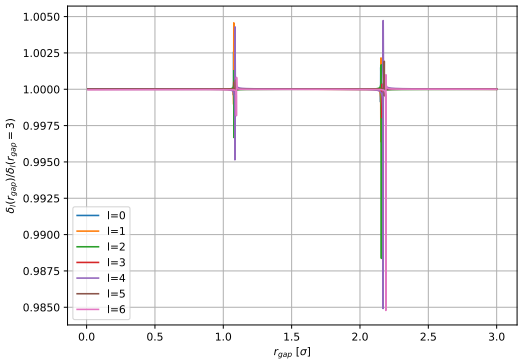

Figure 23: Relative variation of the phase shifts evaluated with respect to the distance between points $r_{gap} = 3\,\sigma$ and $r_{gap} \in [0.1\,\sigma, 3\,\sigma]$.

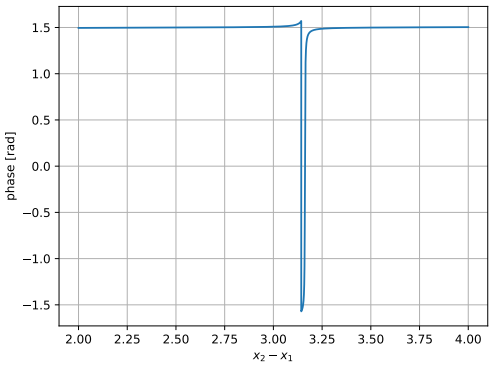

Figure 24: A peak in the evaluation of the phase of a sine function using the method of eq. (6).

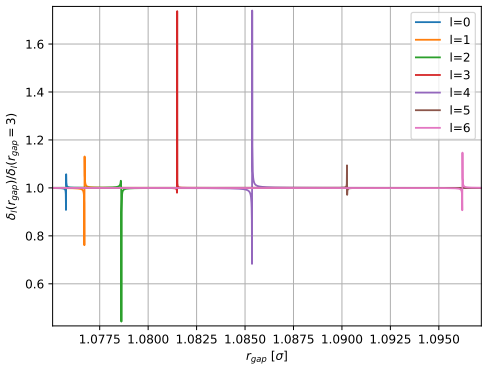

Figure 25: Zoom on the peaks. This figure has been realized using $h = 10^{-5}$ only to have a higher resolution, this does not affects the position of the peaks.

3.7 Point 7

Now we are ready to obtain is the total cross section σ_{tot}. First we have calculated σ_{tot} using eq. (5) and using only the partial waves with angular momentum up to $l = 6$. The results are plotted in fig. 26.

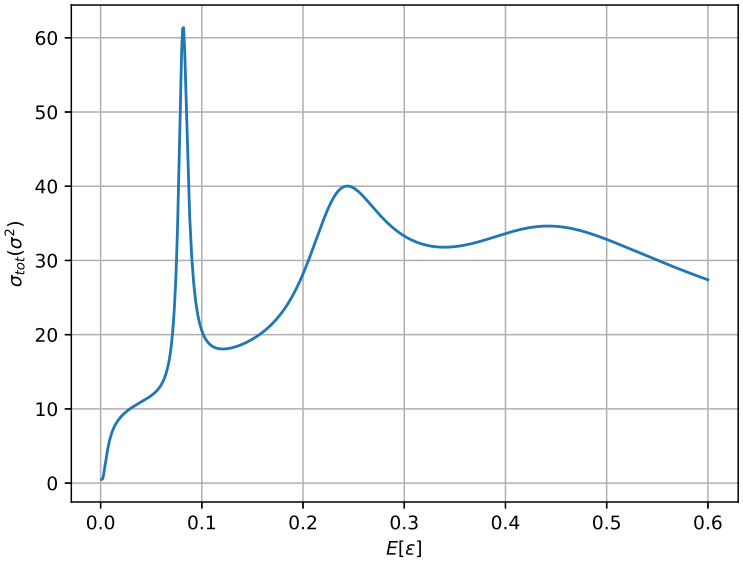

Figure 26: Total cross section σ_{tot} as function of the relative energy E. Notice that axis are in natural units, i.e. as functions of ε and σ.

As we can see from fig. 26, σ_{tot} has three peaks at some values of energy close to 0.1ε, 2.5ε, 4.5ε. We can explain these resonances if we look at the effective potential V_{eff} (fig. 27).

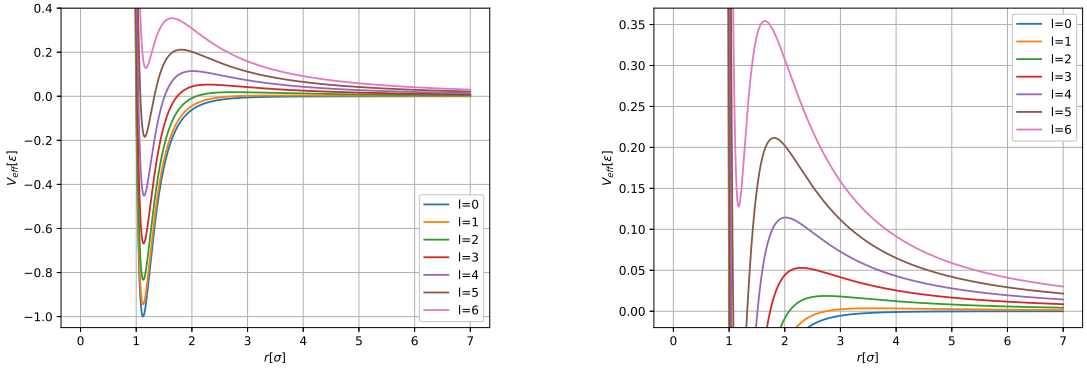

Figure 27: Plot of the effective potential V_{eff} as function of the the relative distance r. Notice that axis are in natural units, i.e. as functions of ϵ and σ.

We have some resonances because the relative[5] incoming particle may be trapped in the well of the effective potential and it can interact with the potential for a longer time, contrarily to a particle that is immediately scattered. This phenomena can happen in two different situations: the relative energy is lower than the peak of V_{eff}, but the particle may tunnel through the potential and then it is trapped inside the potential well. These kind of states are called quasibound resonant states. Instead if the relative energy is higher than the peak of V_{eff}, the particles reaches the potential well but may trapped anyway.

[5] For relative we mean the particle that represents the relative motion of the atoms of H and Kr.

These states are called virtual quasibound states.

What we said can be directly seen in fig. 28 and fig. 29: we see that the wavefunction is higher inside the potential well. We see that the first peak correspond to a quasibound states, while the two other states correspond to two virtual quasibound states.

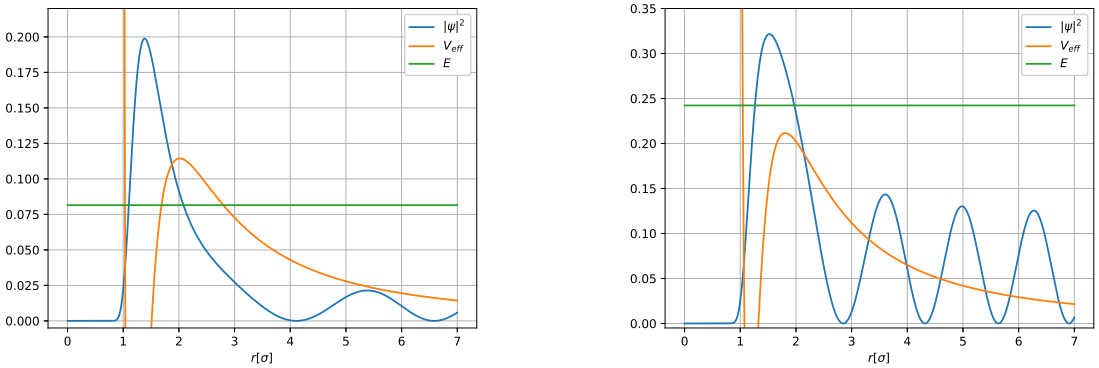

Figure 28: Plots of the modulus square of the wave functions compared to the effective potential. On the left we have the resonant state corresponding to the first peak and on the right the resonant state corresponding to the second peak.

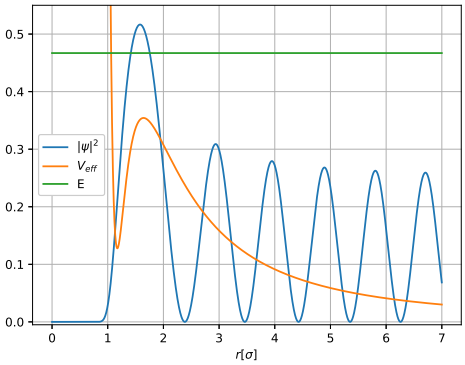

Figure 29: Plot of the modulus square of the wave function compared to the effective potential for the resonant state corresponding to the third peak.

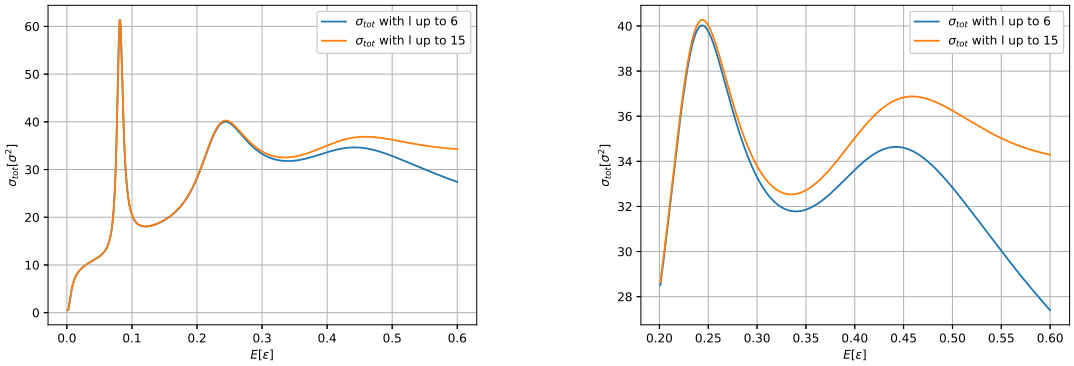

Figure 30: On the left plot of the cross sections considering the contribution of the partial waves up to $l = 6$ and $l = 15$. On the right zoom of the plot where the difference is significant. Notice that axis are in natural units, i.e. as functions of ε and σ.

For the moment we have considered only the partial waves with angular momentum up to $l = 6$. We can see how good is this approximation in fig. 30. As we can see, we do not have significant differences between the two calculated cross section up to $E = 0.2\,\varepsilon$. After $E = 0.2\,\varepsilon$ the difference between the two cross sections is noticeable. This, though, is to be expected: when we consider higher energies, partial waves corresponding to higher momentum starts to become relevant for the scattering experiment. We can expect to obtain a correct cross section with few partial wave contributions only at very low energies. Moreover what is very important is that we do not have more resonances for the energy range that we are studying: even if we do not get the correct cross section at the higher energy, we can consider only the lowest partial waves if we want to study the resonances.

Now we shall study the resonances states better. In particular we are interested at determining the energy of the resonant states and if our model gives the same results of the experimental data. In order to do so we have zoomed our previous plot and we run the algorithm with a higher energy resolution. The plot of the 3 peaks are in fig. 31 and fig. 32.

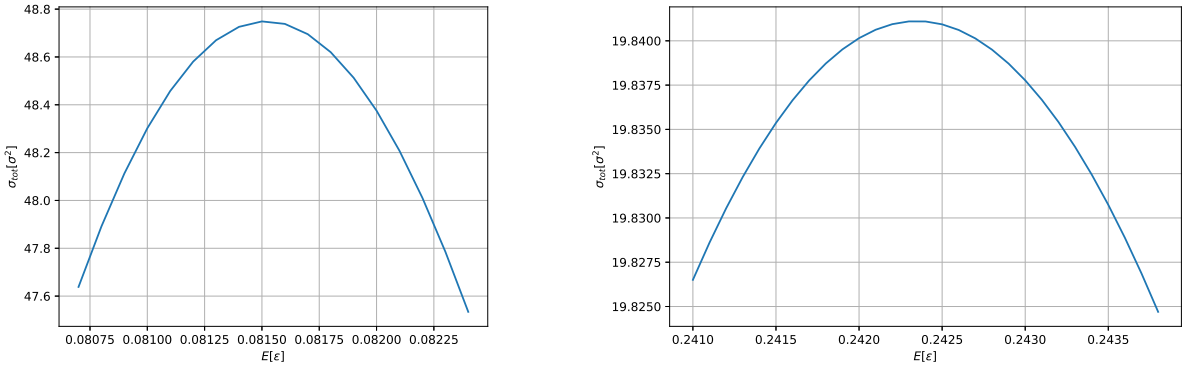

Figure 31: On the left zoom on the first peak plot of the cross sections considering only $l = 4$. On the right zoom on the second peak plot of the cross sections considering only $l = 5$. Notice that axis are in natural units, i.e. as functions of ϵ and σ.

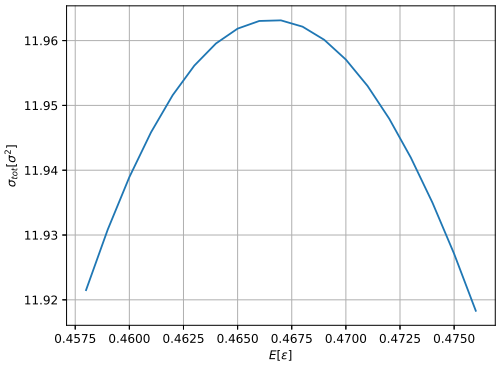

Figure 32: Zoom on the third peak plot of the cross sections considering only $l = 6$. Notice that axis are in natural units, i.e. as functions of ϵ and σ.

We get that the positions of the peak correspond to $E = 0.0815\,\varepsilon, 0.2423\,\varepsilon, 0.467\,\varepsilon$. We can compare these results with the one obtained experimentally[2], but we have to abandon the natural units we adopted and use meV instead (table 2).

Experimental result [meV]	Simulation result [meV]
0.50 ± 0.02	0.48
1.59 ± 0.06	1.43
2.94 ± 0.12	2.76

Table 2: Comparison between numerical results for the energies of the quasibound states and the experimental data.

As we can see from table 2, the energies of the resonances from the theoretical model are systematically lower, but they are compatible with the experimental results within 1, 3 and 2 σ (respectively for the first, second and third peak). Anyway we take into account the fact that we are not considering any error in the theoretical values, therefore the agreement between the experimental results and our simulation would be even better.

Lastly we compare the total cross section σ_{tot} obtained experimentally[6] and the one we obtained from the simulation (fig. 33).

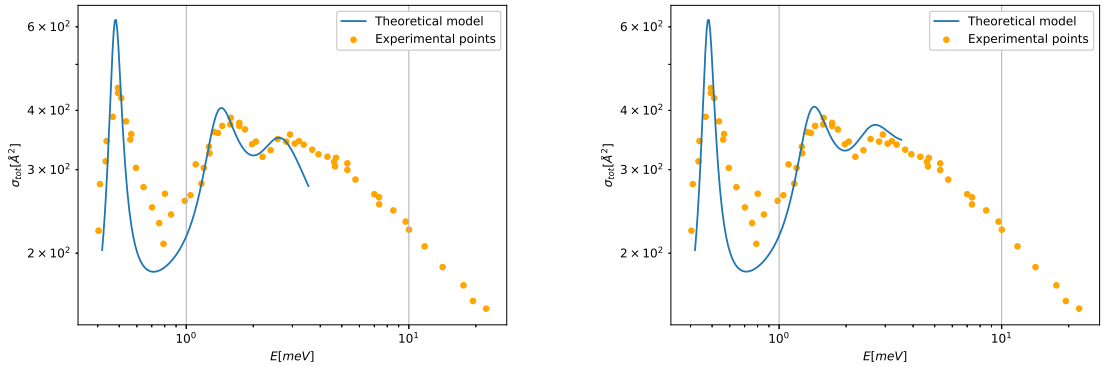

Figure 33: Comparison of the cross section of the theoretical model and the experimental data[2]. On the left the cross section is calculated with partial waves up to $l = 6$, while on the right it is calculated up to $l = 15$.

We clearly see from fig. 33 that the theoretical total cross section σ_{theo} have the same behaviour of the experimental data. However our model is not able to predict correctly the heights of the peaks and, as already said, the peaks are a bit shifted on the left. As expected, if we use the cross section with all the partial waves up to $l = 6$, our model do not follow the experimental data at high energies. Instead if we consider more partial waves we are able to predict the cross section at higher energies.

[6]The experimental data were taken from the original article by hand, therefore they do not correspond to the original data perfectly. Anyway, we wanted to show a qualitatively comparison, so it is not a big deal.

4 Conclusions

We were able to study the bound states of an harmonic potential in 1D and in 3D. In both cases our code was able to calculate the correct wave functions and energies of the bound states. We found out that it is hard to find the optimal mesh step h if we look at the error on the wave functions: the error changes of orders of magnitude for little changes of h and the method is not stable. Moreover the optimal h seems to depend on the energy of the bound state. Anyway, it seems that h of the order of 10^{-2} gives the best result. A more stable method is looking at the errors on the energies. In both cases we can see clearly that h decreases as a power law (a line in a loglog plot). We found out that the exponent of the power law is almost equal 4, that is the order of the error that we expect in the Numerov algorithm. However in the 3D case for $l = 0,\ l = 1$ we find a lower or an higher exponent, respectively. The error then reaches a minimum and start to increase after, because the error due to the loss of numerical precision starts to become dominant. The optimal value of h obtained in this way is equal to 10^{-3}.

Later we studied the total cross section of two particles that interact through a Lennard-Jones potential. We found that the phase shifts δ_l do not depend significantly on the position of the initialization of the wave function and the two points r_1 and r_2 used to calculate δ_l, if these points are chosen accordingly. We see that the phase shifts change a bit if we initialise the wave function too far away from the origin or when the points r_1 and r_2 are too close to the origin.

The total cross section of our model has the same behaviour of the experimental one[2], but it does not follow the experimental data. We were able to predict correctly the presence of three peaks, due to three quasibound states. Moreover we were able to predict the energies of the three resonances correctly: our energy values are all compatible within 3 sigma with the experimental data, but they are all systematically lower.

Appendix A Code and data depository

The data were simulated using C++, while the plots and the data analysis were made in Python. The code written for simulating the data of this report is available at the link `https://github.com/FrancescoSlongo/Computational-Physics---Trento/tree/master/Project_1`.

References

[1] F. Pederiva. *Numerical Solution of the Schrödinger's Equation; Lecture notes for the Advanced Computational Physics Course*. University of Trento, 2020.

[2] J. Peter Toennies, Wolfgang Welz, and Günther Wolf. *Molecular beam scattering studies of orbiting resonances and the determination of van der Waals potentials for H–Ne, Ar, Kr, and Xe and for H2–Ar, Kr, and Xe*. J. Chem. Phys. 71, 614 (1979)